RSC Advances

PAPER

Cite this: *RSC Adv.*, 2021, **11**, 34291

Tb^{3+}-Doped Ag-MOFs for fluorescent detection of formaldehyde in a novel smartphone platform and its removal applications in milk products and wastewater†

Mengwen Li,[a] Ao Shen,[a] Man Du,*[b] Xiaohui Hao,[a] Hongquan Wang,*[c] Xiaoyu Du,[a] Shufeng Ma,[a] Jiaxin Yuan[a] and Yunxu Yang *[a]

Received 2nd August 2021
Accepted 25th September 2021

DOI: 10.1039/d1ra05856h

rsc.li/rsc-advances

As one kind of reactive carbonyl species (RCS), formaldehyde (FA) with a high concentration could be extremely toxic to living bodies as well as the environment. This paper reports a three-dimensional (3D) Tb^{3+}@Ag-MOFs-based fluorescent probe for fast sensing of FA, which uses a novel turn-on mechanism based on the luminescence induced by Tb^{3+}. The MOF sensor shows broad dynamic ranges of 0.1–1 mM for FA with the detection limit of 1.9 μM. For online and real-time detection of FA, a portable smartphone platform was employed to analyze the RGB values of the fluorescence by a smartphone application. By incorporating this probe into a polyacrylonitrile (PAN) layer, we synthesized a film composite that could effectively remove FA in real samples including milk and chemical factory wastewater, and the removal rate reached 98.52% and 95.38% respectively. Moreover, the potential of the film to remove gaseous FA was confirmed by experiments as well.

1 Introduction

Over the years, the recognition and removal of aldehydes have always drawn great attention and discussion due to their biological toxicity.[1–3] Among these aldehydes, formaldehyde (FA) is harmful to public health and the environment. Such a colorless, volatile and deleterious substance can cause the eyes discomfort as well as causing asthma and respiratory infection.[4] Therefore, FA is classified as a primary carcinogen. As such, it's important to detect and remove FA in the diet and environment safely and efficiently.

Considering its significance, novel sensors for FA with simplicity, low cost, a low limit of detection, instantaneous response and high removal rate at room temperature should be developed as soon as possible. Current measures for detecting FA mainly include gas chromatography,[5] high-performance liquid chromatography,[6] and spectrometry,[7] which offer high selectivity and sensitivity but are expensive, time consuming and difficult in terms of operation. Considering the reactivity and high volatility of FA, the methods based on fluorescent probes have obvious advantages like short trapping time, high selectivity and sensitivity, and easy to achieve *in situ* and real time imaging.[8–15]

On the other hand, metal organic frameworks (MOFs) as a novel kind of sensors for FA has aroused huge attention due to its good performance. Compared with other materials and methods, MOFs materials have turnable functionality, rich pores, outstanding stability and conjugated skeleton.[16–21] Currently, only several MOFs probe have been developed for the fluorescent detecting of FA (Table S1†).[22–26] However, the response time and detection limit of some MOF materials to FA are not good enough, and some of them can only detect FA in aqueous-phase but not vapor-phase. Lanthanide MOFs (Ln-MOFs), as a subfamily of MOF, possess lots of excellent luminescence properties, including large quantum yields, sharp-line emissions, and long luminous life. Therefore, Ln-MOFs have been employed in luminescent materials and sensing for ions and small molecules.[27–37]

Herein, we proposed a novel turn-on mechanism for FA sensing based on "self-assembly of MOF structure" and "antenna effect of Tb^{3+}". To fulfill this purpose, the metal ion vertex of MOF probe should be able to react with FA sensitively to make MOF collapse and release free ligands. Meanwhile, there should be an antenna effect between the ligands and Tb^{3+} to turn on fluorescence response, and the ligands should not contain any other extra functional groups as well, which would react with FA and produce unnecessary interference. Thus,

[a]*Department of Chemistry and Chemical Engineering, School of Chemistry and Biological Engineering, University of Science and Technology Beijing, Beijing 100083, China. E-mail: yxyang@ustb.edu.cn*

[b]*School of Chemical and Pharmaceutical Engineering, Hebei University of Science and Technology, Shijiazhuang, 050018, China. E-mail: mandu@hebust.edu.cn*

[c]*State Key Laboratory of Pathogen and Biosecurity, Beijing Institute of Microbiology and Epidemiology, Beijing, 100071, China. E-mail: bjwanghq@163.com*

† Electronic supplementary information (ESI) available. See DOI: 10.1039/d1ra05856h

a probe of **Tb^{3+}@Ag-BTC** was designed and synthesized in order to verify the above mechanism (BTC, 1,3,5-benzenetricarboxylic acid) as shown in Scheme 1a. Indeed, when the detection reaction began between **Tb^{3+}@Ag-BTC** and FA, Ag^{+} vertexes were reduced to Ag^{0} by FA, and Tb^{3+} was sensitized with energy by the released ligands (BTC) in $\lambda_{ex} = 365$ nm at the same time, which showed characteristic green fluorescence. On the other hand, the fluorescent test papers had been prepared for a smartphone sensing platform so that we could analyze the R, G and B channel values transmitted from a spectrophotometer to the smartphone's APP by bluetooth (Scheme 1b). Additionally, **Tb^{3+}@Ag-BTC** could easily be modified to make a thin-film nanocomposite by dispersed it into PAN in order to remove the FA in milk and chemical factory wastewater. So, with the nanoscale **Tb^{3+}@Ag-BTC**, we were able to realize the sensitive detection of FA and provide a new tool for FA removal.

2 Experimental section

2.1 Materials and instrumentations

All the details of materials, reagents and instruments were shown in ESI.†

2.2 Synthesis of Tb^{3+}@Ag-BTC

Ag-BTC was synthesized according to existing reports (Scheme S1†).[38] Ag-BTC (0.53 g, 1 mmol) was dispersed into 50 mL DMF in a 100 mL round-bottomed flask by ultrasonic treatment for 15 min, then a DMF solution of $TbCl_3 \cdot 6H_2O$ (0.37 g, 1 mmol) was dropped in. The mixture was stirred for 48 h at 25 °C, after which the particles were filtered by vacuum filtration and washed with methanol (25 mL × 3). The obtained **Tb^{3+}@Ag-BTC** sample was soaked into 50 mL acetone under string for 24 h to remove the rest $TbCl_3 \cdot 6H_2O$, and then dried at 70 °C for 6 h at air atmosphere.

2.3 Preparation of Tb^{3+}@Ag-BTC@PAN film

Firstly, 1.5 g PAN was dissolved in 15 mL DMF and heated to 80 °C for 48 h, then cooled to room temperature. Secondly, the synthesized **Tb^{3+}@Ag-BTC** (0.5 g) was add into above PAN solution forming a suspension. At last, the suspension was evenly dropped into a round Petrie dish (5 cm in diameter), after which the Petrie dish was immersed in deionized water for 30 s to obtain the **Tb^{3+}@Ag-BTC@PAN** film.

2.4 Fluorescence sensing of FA

The stock solutions of FA with different concentrations (0.1–1.2 mM) were prepared in deionized water, and 25 mL stock solution of **Tb^{3+}@Ag-BTC** (4 mM, 1.7 mg mL^{-1}) was prepared in DMF and Tris buffer (7 : 3, v/v). Excitation wavelength was 365 nm and emission slit widths was 5.0 nm and 10.0 nm separately. The fluorescence spectra were scanned and collected from 450 nm to 650 nm at 1200 nm min^{-1}.

2.5 Specific detection

In order to verify the specificity of **Tb^{3+}@Ag-BTC** for detecting FA, another nine common substances harmful to food and the environment were employed as comparisons, including acetaldehyde, trichloroacetaldehyde, acetamide, acrylonitrile, trichloromethane, diethanolamine, melamine, Pb^{2+} and Hg^{2+}. All the analytes (1 mM) were incubated with **Tb^{3+}@Ag-BTC** suspension for 15 min respectively, after which the fluorescence spectra of these nine mixtures were collected from 450 nm to 650 nm with the excitation of 365 nm.

2.6 Preparation of test papers for smartphone sensing

Clean blank neutral fliter papers (1 cm × 3 cm) were soaked in a **Tb^{3+}@Ag-BTC** suspension (4 mM, 1.7 mg mL^{-1}) for 10 min, and then taken out and dried at 70 °C in a drying oven. This process was cycled three times for obtaining the test papers.

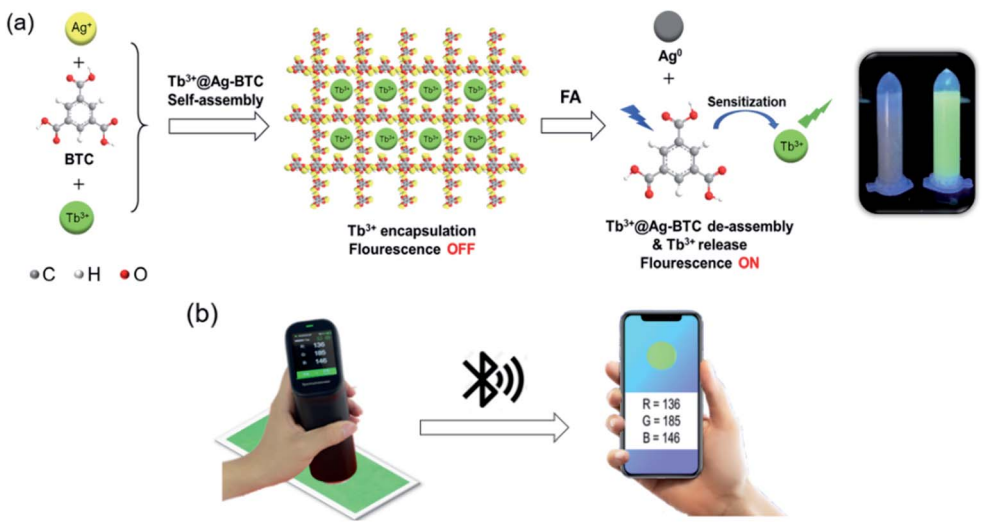

Scheme 1 (a) Schematic representation of nanoscale **Tb^{3+}@Ag-BTC** for fluorescent FA sensing. (b) The detection of test paper on a smartphone platform.

Subsequently, the test papers were coated with different concentrations of FA solutions (0.1–1 mM) respectively and incubated for 3 min, then placed under the spectrometer one by one for smartphone sensing.

2.7 Preparation of real samples

In order to evaluate the **Tb^{3+}@Ag-BTC@PAN** film as real samples, pure milk was purchased from the local market and pretreated according to the previous report to remove the proteins and other organic substances.[39] In brief, 0.45 g trichloroacetic acid was added into 10 mL milk product in a round-bottomed flask under the stirring for 10 min. After observing the white precipitate, stirring was stopped and the flask was stand for 2 min. At last, the precipitate was filtrated by the vacuum filtration and the filtrate was used for practical applications. 10 mL wastewater from chemical factory were diluted 20 times with deionized water. Besides, FA (0.1 mM, 10 mL) was added into above samples respectively for the removal application.

3 Results and discussion

3.1 Characterization of Tb^{3+}@Ag-BTC

As a known MOF material, the structural characterizations of Ag-BTC, including PXRD, FT-IR spectra, XPS, SEM and *et al.*, have been reported.[40] Based on the existing research, we also characterized the structure of Ag-BTC doped with Tb^{3+}, and compared **Tb^{3+}@Ag-BTC** with Ag-BTC to further illustrate its structure.

Fig. 1 showed that the PXRD peaks of **Tb^{3+}@Ag-BTC** composites contained the peaks of Ag-BTC and those of terbium species. All the results above indicated that **Tb^{3+}@Ag-BTC** possessed a good crystal form and the similar crystal structure as Ag-BTC.

In Fig. 2, FT-IR spectra provided some qualitative information about BTC, $TbCl_3 \cdot 6H_2O$, Ag-BTC and **Tb^{3+}@Ag-BTC**. In the spectrum of ligand BTC, the peaks of –OH and C=O appeared at 3090, 1717 and 1600 cm^{-1} respectively (black curve). After coordinated with Ag^+, they moved to 3300, 1621 and 1555 cm^{-1} (green curve). On the red curve, the peaks at 2232 and 2030 cm^{-1} represented Tb^{3+} which could be seen obviously on the spectrum of **Tb^{3+}@Ag-BTC** as well (blue curve). Furthermore, it was worth mentioning that the peaks of C–H and C–C in BTC ligand had no obviously change compared with those of Ag-BTC and **Tb^{3+}@Ag-BTC** because of the bonds of C–H and C–C were not involved in coordination. Thus, **Tb^{3+}@Ag-BTC** belongs to the same series of Ag-BTC in morphology.

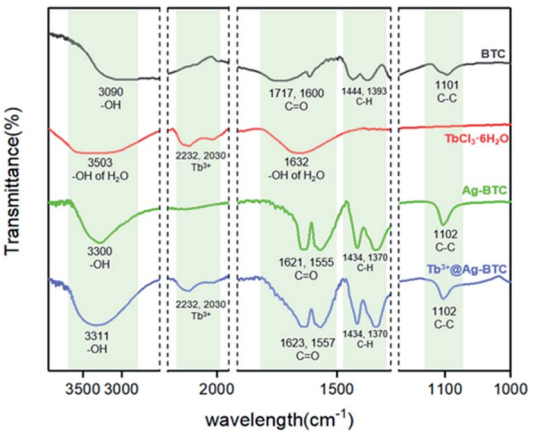

Fig. 2 FT-IR spectra of BTC (black curve), $TbCl_3 \cdot 6H_2O$ (red curve), Ag-BTC (green curve) and **Tb^{3+}@Ag-BTC** (blue curve).

The morphology characterizations of Ag-BTC and **Tb^{3+}@Ag-BTC** were characterized by SEM test. As shown in Fig. 3a and b, Ag-BTC had a very regular morphology and a typical nano-stick appearance. While in Fig. 3c and d, Ag-BTC nano-sticks were surrounded with Tb^{3+} particles but were still kept the initial morphology, which indicated Tb^{3+} was loaded in Ag-BTC successfully.

In Fig. 4, thermogravimetric analysis (TGA) of **Tb^{3+}@Ag-BTC** was carried out in the air from 50–800 °C to research its thermal stability. According to the TG curve, **Tb^{3+}@Ag-BTC** showed excellent thermal stability at 278 °C in the air atmosphere. The slight weight loss of 1.9 wt% in 103–278 °C could be owing to the separation of guest solvent molecules in MOF holes. The

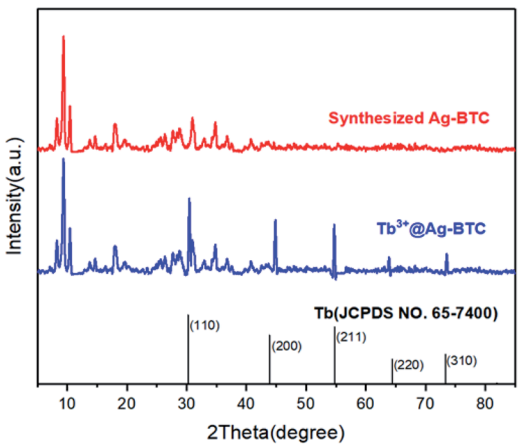

Fig. 1 PXRD pattern of the synthesized Ag-BTC, **Tb^{3+}@Ag-BTC** and Tb sample (JCPDS No. 65-7400).

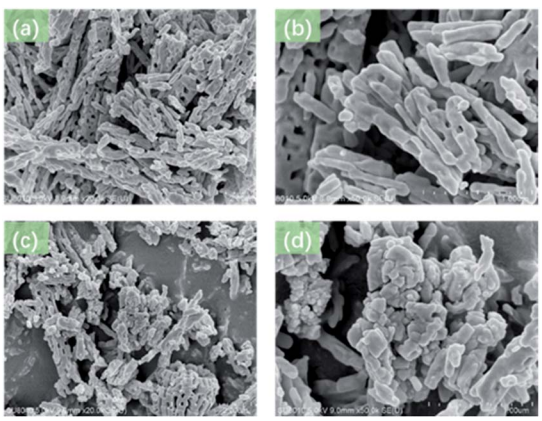

Fig. 3 (a and b) SEM of Ag-BTC. (c and d) SEM of **Tb^{3+}@Ag-BTC**.

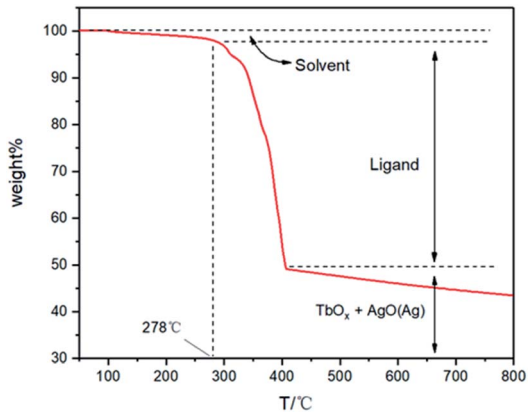

Fig. 4 Thermogravimetric analysis (TGA) of **Tb^{3+}@Ag-BTC** in an air atmosphere in 50–800 °C with a heating rate of 10 °C min^{-1}.

considerable weight loss of 48.1 wt% in 278–408 °C could be attributed to the decomposition of BTC ligands from the framework and the MOF structure started to decompose. After 408 °C, Ag^+ and Tb^{3+} formed their oxides in the air atmosphere with high temperature. While, AgO will gradually decompose to release oxygen with the temperature continuously rising, so the final curve showed a downward trend.

N_2 sorption studies of **Tb^{3+}@Ag-BTC** were also carried out to illustrate its microporosity. It could be seen in Fig. 5, **Tb^{3+}@Ag-BTC** comforted to the type-I N_2 sorption isotherms, which belonged to a kind of typical microporous material. Further data showed the BET surface area was 10.87 m^2 g^{-1} (p/p^0 = 0.30), micropore volume was 0.02 cm^3 g^{-1} (p/p^0 = 0.99) and average pore size was 6.83 nm.

3.2 Research on the influence of pH

The effects of pH for FA detection were also studied. **Tb^{3+}@Ag-BTC** (4 mM, 1.7 mg mL^{-1}) and FA (1 mL) were dispersed in 25 mL of DMF and Tris buffer solution (7 : 3, v/v), and sonicated for 5 min. Since the MOF structure of the probe would collapse in an acidic environment, the fluorescence intensity was only

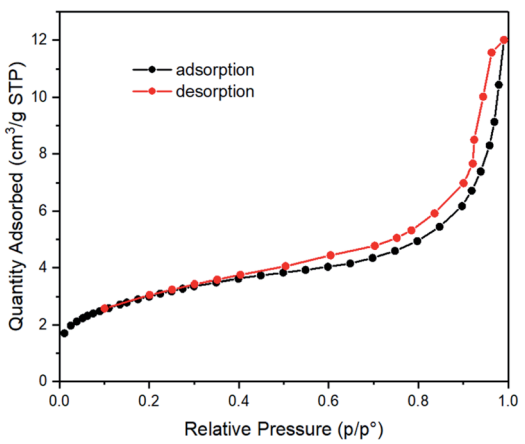

Fig. 5 N_2 adsorption (black curve) and desorption (red curve) isotherms of **Tb^{3+}@Ag-BTC** recorded at −195.8 °C.

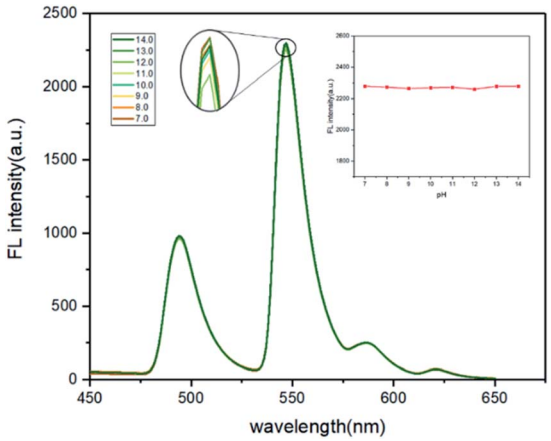

Fig. 6 The fluorescence intensity changes of **Tb^{3+}@Ag-BTC** response to FA in different pH. **Tb^{3+}@Ag-BTC** was 4 mM (1.7 mg mL^{-1}), FA was 1 mM, in DMF and Tris buffer solution (7 : 3, v/v), λ_{ex} = 365 nm.

measured in different pH ranges from 7.0 to 14.0. Tris buffer solution and pH meter were used for the adjustment and monitoring of pH values respectively. The results demonstrated that the pH value had little effects on the fluorescence intensity (Fig. 6). Therefore, the prepared probe dispersions were directly used without adjusting in the later detections.

3.3 Fluorescent determination for FA

Fluorescence titration experiments were carried out to investigate the response of **Tb^{3+}@Ag-BTC** to different concentrations of FA (Fig. 7). Studies of the fluorescence spectra showed that after sensitized by released BTC, the characteristic sharp-line emissions of Tb^{3+} were exhibited at 494 nm, 547 nm, 587 nm, and 622 nm under the excitation at 365 nm. The maximum emission at 547 nm owed to the $^5D_4 \rightarrow {}^7F_5$ hypersensitive transition. In Fig. 7, the fluorescence intensity was increased evenly with the addition of FA from 0.1 to 1.2 mM. At the same

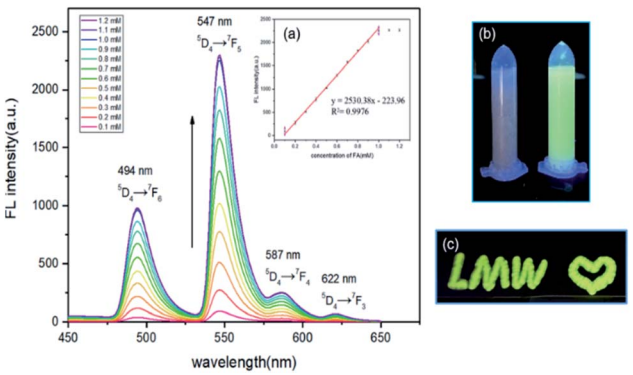

Fig. 7 The fluorescence intensity of **Tb^{3+}@Ag-BTC** in different FA concentrations. (a) The linear fit of the fluorescence intensity upon FA concentrations. (b) The fluorescence color change of **Tb^{3+}@Ag-BTC** before and after response to FA under UV lamp. (c) Fluorescent characters written on a silicone glass plate. **Tb^{3+}@Ag-BTC** was 4 mM (1.7 mg mL^{-1}), FA was 0.1–1.2 mM, in DMF and Tris buffer (7 : 3, v/v), pH = 7.0, λ_{ex} = 365 nm.

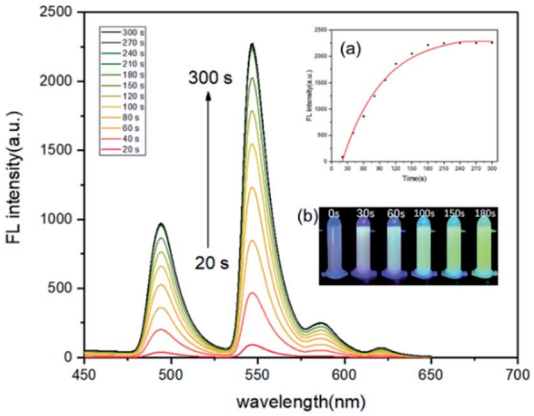

Fig. 8 Fluorescence signaling of Tb^{3+}@Ag-BTC to FA from 20 s to 300 s. Inset: (a) Kinetic plot of Tb^{3+}@Ag-BTC to FA. (b) The fluorescence color change at different time under UV lamp. Tb^{3+}@Ag-BTC was 4 mM (1.7 mg mL^{-1}), FA was 1 mM, in DMF and Tris buffer (7 : 3, v/v), pH = 7.0, λ_{ex} = 365 nm.

time, the fluorescence color of **Tb^{3+}@Ag-BTC** changed from colorless to green (Fig. 7b). Through the linear fit of the fluorescence intensity from 0.1 to 1 mM of FA concentrations, there existed a excellent linear relationship ($R^2 = 0.9976$). The lowest detection limit was calculated to be 1.9 μM by the equation $L_{OD} = 3\delta/m$ (Fig. 7, inset a).

3.4 Research on response time

For the time-dependence study, 4 mM (1.7 mg mL^{-1}) **Tb^{3+}@Ag-BTC** and 1 mM FA were added into the DMF and Tris buffer, and the fluorescence spectra were recored from 20 s to 300 s. Fig. 8 showed that the fluorescence intensity reached its maximum at 180 s and remains stable (Fig. 8, insert a), which was about 25 times greater than that at 20 s. It revealed that the response time of probe to FA was 180 s. The pseudo-first-order rate constant (k') was calculated to be 0.66 min^{-1} by kinetic study (Fig. S3†). Above results demonstrated that **Tb^{3+}@Ag-BTC** could detect FA quantitatively, and expressed a fast response time by the fluorescence method.

Furthermore, in order to eliminate the interference of environmental factors, mainly including O_2 and temperature within this 180 s, we had made the following supplements and explanations: (1) before the recognition of **Tb^{3+}@Ag-BTC** to FA solution, the container had been pretreated by vacuum, and the entire recognition process was carried out in a closed nitrogen atmosphere. Therefore, the interference of O_2 could be eliminated. (2) We carried out recognition experiments of **Tb^{3+}@Ag-BTC** for FA at different temperatures (10–40 °C). In Fig. S4,† the fluorescence spectra at other temperatures were consistent with the results we measured at 25 °C, which illustrated **Tb^{3+}@Ag-BTC** was a stable probe for FA and would not be disturbed by the environmental.

3.5 Selectivity of Tb^{3+}@Ag-BTC toward FA

The selectivity to the analyte is an essential indicator of a fluorescent probe. Therefore, we explored the selectivity of **Tb^{3+}@Ag-BTC** to FA compared with a series of common harmful analytes (acetaldehyde, trichloroacetaldehyde, acetamide, acrylonitrile, trichloromethane, diethanolamine, melamine, Pb^{2+}, Hg^{2+}, acetone, propionaldehyde, acetonitrile, benzaldehyde and phenol). From Fig. 9, it became obvious that the fluorescence intensity of the probe had no obvious change with other analytes. On the contrary, FA could enhance the fluorescence intensity of **Tb^{3+}@Ag-BTC**, which demonstrated that **Tb^{3+}@Ag-BTC** was able to detect FA selectively.

3.6 Mechanism of FA sensing

As one of the typical rare earth elements, Tb^{3+} has sharp, line-like emission and longlived luminescence. Unfortunately, under the influence of the parity forbidden f–f transitions, the luminescent intensity of Tb^{3+} is weakly. On the other hand, with the coordination with organic ligands, especially aromatic compounds rich in carboxyl groups,[41] Tb^{3+} will be sensitized and produce strong luminescence (the "antenna effect"), namely the excited ligands molecules will nonradiative transfer the energy to the $^7F_5$ states of Tb^{3+} ions.

It is a well-known reaction that Ag^+ can oxidize the aldehyde group and is itself reduced to Ag^0.[42] This is due to the fact that $E^0_{(Ag^+/Ag)}$ is 0.77 V, $E^0_{(HCOOH/HCHO)}$ is −0.03 V, which the former is higher than the latter. Thus, the oxidizing of Ag^+ was

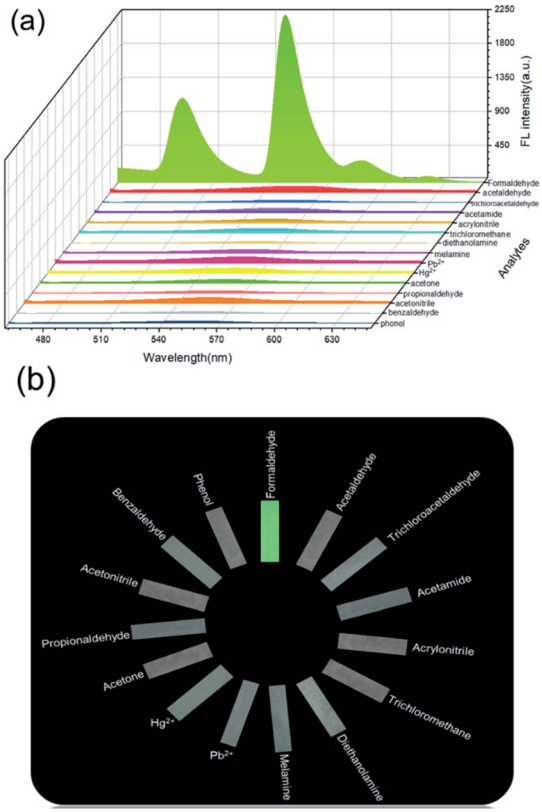

Fig. 9 (a) Fluorescence intensity of Tb^{3+}@Ag-BTC in different analytes. (b) Fluorescence test papers of various analytes taken under 365 nm UV lamp in selective testing. Tb^{3+}@Ag-BTC was 4 mM (1.7 mg mL^{-1}), analytes were 1 mM, in DMF and Tris buffer solution (7 : 3, v/v), pH = 7.0, λ_{ex} = 365 nm.

stronger than FA, and Ag^+ could be reduced by FA as displayed in eqn (1)–(4). Indeed, the Ag^+ metal sites in the Ag-MOF should be reduced by FA from Ag^+ to Ag^0 and the MOF structure would collapse consequently. Besides, we could also see with naked eyes that Ag^0 was formed after **Tb^{3+}@Ag-BTC** reacted with FA (Fig. S6†), and the XPS test also showed out the precipitate of Ag element (Fig. S7†). Meanwhile, the released BTC ligand would coordinate with Tb^{3+} and transfer the energy to Tb^{3+} at an excitation of 365 nm, which called photoinduced electron transfer (PET). Thus, the turn-on green fluorescence was clearly observed, thereby enabling the detection of FA (Scheme 2). The procedure could be depicted as eqn (1)–(4).

$$Ag^+ + HCHO \rightarrow Ag_{(s)} + HCOOH \quad (1)$$

$$TBC + Tb^{3+} \rightarrow Tb^{3+}\text{–TBC fluorescent product} \quad (2)$$

$$Ag_{(aq)}{}^+ + e^- \leftrightharpoons Ag_{(s)},\ E^0 = 0.77\ V \quad (3)$$

$$HCOOH_{(aq)} + 2e^- \leftrightharpoons HCHO_{(aq)},\ E^0 = -0.03\ V \quad (4)$$

In order to prove that FA was oxidized to formic acid by Ag^+ after the reaction between **Tb^{3+}@Ag-BTC** and FA, the oxidation product was extracted by organic solvent and used for ^1H NMR identification. The characteristic H peaks of formic acid was detected, which illustrated FA was oxidized to formic acid by Ag^+ (Fig. S8†). ^1H NMR (400 MHz, D_2O) d (TMS, ppm): 8.05 (s, 1H), 12.6 (s, 1H).

On the other hand, ^1H NMR and ESI mass tests of the released ligand (BTC) were employed (Fig. S5a and b†). ^1H NMR (400 MHz, DMSO-d_6) δ (TMS, ppm): 8.89 (s, 3H), 12.74 (s, 3H). ESI(+)-HRMS (m/z): for TBC: calcd, 210.08, found: [M], 210.02, $[M + H]^+$, 211.02. In addition, FT-IR spectra of Tb-BTC was carried and compared with BTC and Tb^{3+}. It could be seen in Fig. 10, the peaks of –OH and C=O of BTC appeared at 3090, 1717 and 1600 cm^{-1} respectively (black curve). While, in the spectrum of response product of Tb-BTC, they moved to 3360, 1615 and 1517 cm^{-1} (red curve), which confirmed that BTC combined with Tb^{3+} and sensitized it. These results suggested that **Tb^{3+}@Ag-BTC** could detect FA on basis of the expected mechanism.

The existence of the antenna effect successfully compensated for the low energy absorption efficiency of Tb^{3+}, and greatly improved the fluorescence ability of Tb^{3+}. The theoretical calculations were performed to confirm this mechanism

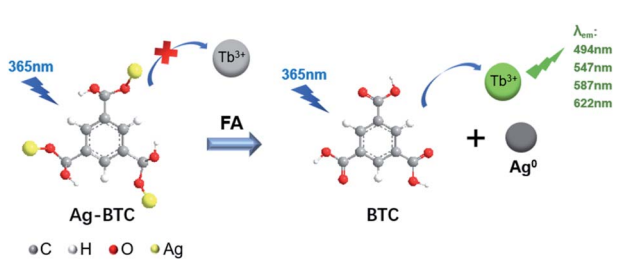

Scheme 2 Proposed mechanism of FA sensing.

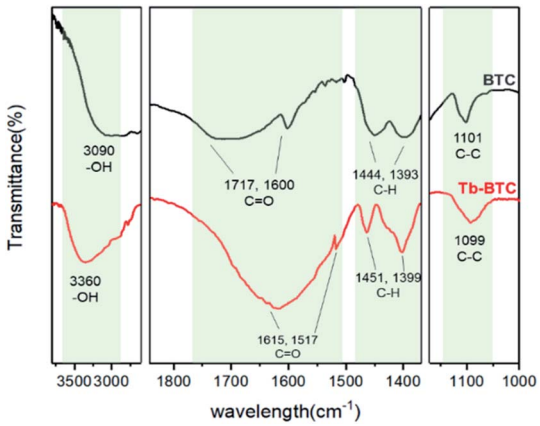

Fig. 10 FT-IR spectra of BTC (black curve) and Tb-BTC (red curve).

which used the B3LYP/6-31G(d) basis set in the Gaussian 09 package. Fig. 11 displayed the optimized molecular structures and the energy gap (ΔE) of HOMO and LUMO of $TbCl_3$ and Tb-BTC. The ΔE of Tb-BTC was 0.81843 eV, which was narrower than that of $TbCl_3$ (2.99025 eV). Therefore, when illuminated by an excitation light source of the same wavelength (365 nm in this work), Tb-BTC was more easily excited and fluoresced than Tb^{3+} ions.

3.7 Smartphone-sensing platform for FA sensing

Fluorescent test papers were prepared for real-time and online detection of FA by smartphone-sensing platform. This portable platform was composed of a UV lamp (λ_{ex} = 365 nm), a smartphone and a spectrophotometer connecting with the smartphone by bluetooth. Once the camera of spectrophotometer captured the fluorescence color of test paper, the smartphone would show a round symbol in same color as the test paper immediately (Fig. 12a). As could be seen in Fig. 12c, with the adding of different FA concentrations, the test papers showed a series of fluorescence changes from colorless to green. Afterwards, a color-read APP (ColorMeter) installed on the smartphone could analyze the fluorescence photos and output the

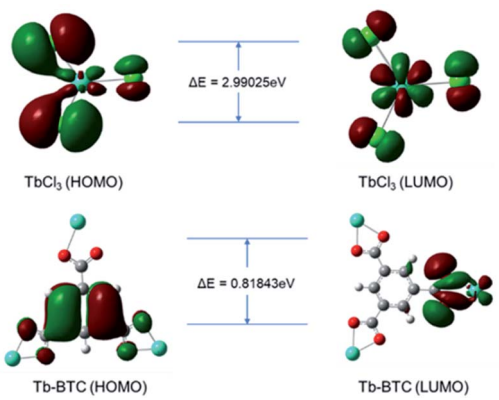

Fig. 11 Molecular amplitude plots the HOMO and LUMO of $TbCl_3$ and Tb-BTC.

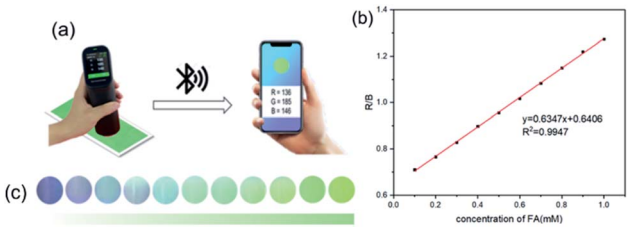

Fig. 12 (a) The RGB analysis for the fluorescence changes of Tb^{3+}@Ag-BTC to FA based on the smartphone. (b) The liner relationship between the B/R values to. (c) The fluorescence changes in different FA concentrations.

corresponding RGB values. Moreover, it was worth noting that the R/B values were highly correlated to FA concentrations. Through the linear fit of 10 data collections, there was an good linear relationship of the R/B values to FA concentrations in 0.1–1 mM ($R^2 = 0.9956$), as shown in Fig. 12b. Lod was calculated to be 1.6 μM, which was slightly lower than 1.9 μM obtained by Hitachi F-4500 Flourescence Spectrophotometer. Thus, this smartphone-sensing platform could realize the real-time and online detection of FA and was provided with higher sensitivity.

3.8 Applications of Tb^{3+}@Ag-BTC@PAN film

The permanent porosity, efficient strong emission and fast response of **Tb^{3+}@Ag-BTC** to FA prompted us to evaluate the detection of FA in practical application. Herein, we designed and fabricated a new polymer-MOF of **Tb^{3+}@Ag-BTC@PAN** which was developed as a luminescent material for FA removal in aqueous solution and in air. The schematic representation of **Tb^{3+}@Ag-BTC@PAN** treated with FA before and after were shown in Scheme 3.

In order to explore the absorption abilities of **Tb^{3+}@Ag-BTC@PAN** film toward FA, the practical applications in some real samples including pure milk and the wastewater from local chemical factory were studied. It was worth mentioning that the ratio of FA concentration and the volume of **Tb^{3+}@Ag-BTC@PAN** film were optimized to obtain the best removal performance (Fig. S11 and S12†). According to the device shown in Fig. 13, three layers of **Tb^{3+}@Ag-BTC@PAN** films were filled into a glass column (5 cm in diameter, 20 cm in height), and the processed samples were added. After 10 minutes, the effluent solutions were collected by the 20 mL glass beakers for GC analysis. According to gas chromatography test results (Tables S2 and S3†),

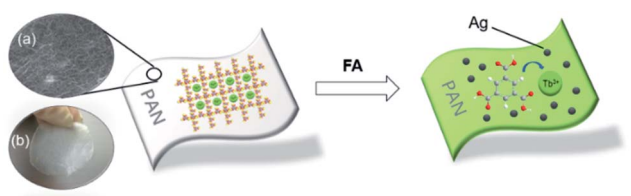

Scheme 3 Schematic representation of Tb^{3+}@Ag-BTC@PAN film treated with FA. (a) SEM of Tb^{3+}@Ag-BTC@PAN film morphology; (b) Tb^{3+}@Ag-BTC@PAN film visible to the naked eyes under natural light.

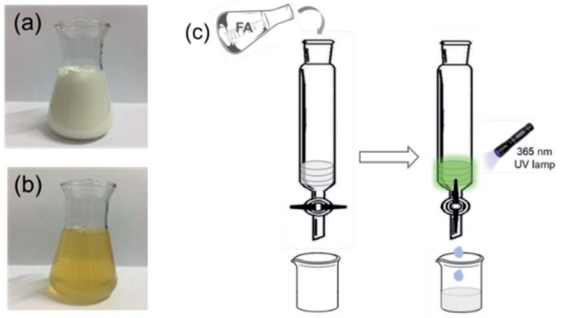

Fig. 13 (a) Pure milk sample. (b) Factory wastewater sample. (c) Device for removing FA in real samples.

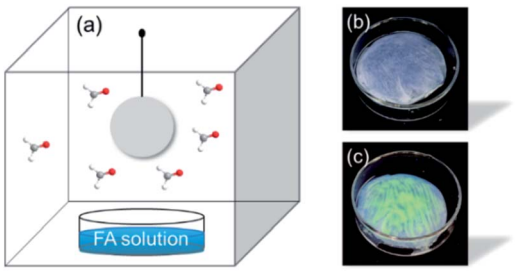

Fig. 14 (a) Device for adsorbing and removing FA gas. FA solution was 0.1 M, 25 °C. (b) and (c) The fluorescence change of the Tb^{3+}@Ag-BTC@PAN film before and after reacting with FA.

Tb^{3+}@Ag-BTC@PAN film could removal the FA in pure milk and factory wastewater samples and the removal rate reached 98.52% and 95.38% respectively. The remaining concentration of FA in real samples were 1.48 μM in pure milk and 4.62 μM in wastewater, which were lower than the lethal dose of FA of 800 mg L^{-1}.[43] In addition, **Tb^{3+}@Ag-BTC** was used to detected FA in milk and wastewater. The experimental details and fluorescence titration spectra were described in ESI (Fig. S9 and S10†). It showed that **Tb^{3+}@Ag-BTC** could detect FA in milk and wastewater and there were the good linear relationships as well.

Besides, in order to explore the feasibility of **Tb^{3+}@Ag-BTC@PAN** in adsorbing and removing gaseous FA, it was put inside a quartz cuvette (25 cm × 25 cm × 30 cm) which contained gaseous FA as analyte (Fig. 14). After 10 min, **Tb^{3+}@Ag-BTC@PAN** film was taken out and placed under a UV lamp to observe the change of fluorescence. It could be seen clearly in Fig. 14b and c, **Tb^{3+}@Ag-BTC@PAN** film produced strong green fluorescence. This positive result indicated that **Tb^{3+}@Ag-BTC@PAN** film we prepared could be used as a convenient and sensitive material for FA removal in air atmosphere.

4 Conclusions

In summary, an ultrasensitive and selective fluorescent probe (**Tb^{3+}@Ag-BTC**) for detecting FA had been developed. As confirmed by the characterization results, **Tb^{3+}@Ag-BTC** showed good thermal stability of 278 °C in the air and the BET surface area was 10.87 m^2 g^{-1}. The proposed MOF sensor

showed good selectivity and rapid enhancement of green fluorescence when exposed to FA. The lowest detection limit towards FA was 1.9 μM in the dynamic range from 0.1 to 1 mM, and the response time was 180 s. Moreover, number of other harmful gases were tested, and none of them gave noticeable interference. The turn-on fluorescence could be attributed to the "self-assembly of MOF structure" and "antenna effect of Tb^{3+}", which confirmed by ^1H NMR and mass analysis. For online and real-time detection of FA, a portable smartphone platform had been employed to analyze the RGB channel values of the fluorescence by a color-read APP. In addition, its polymer-MOF film (**Tb^{3+}@Ag-BTC@PAN**) had been designed for removing the FA in aqueous and gaseous. Surprisingly, the removal rate could reach 98.52% and 95.38% in pure milk and chemical factory wastewater. **Tb^{3+}@Ag-BTC@PAN** film also had the considerable ability for removing gaseous FA. All in all, this research reported a novel functional MOF probe and a new smartphone platform for the sensitive, selective and real-time detection of FA, as well as its removal applications in real samples.

Author contributions

Mengwen Li: conceptualization, writing – original draft. Ao Shen: validation. Man Du: conceptualization. Xiaohui Hao: investigation. Hongquan Wang: project administration. Xiaoyu Du: software. Shufeng Ma: resources. Jiaxin Yuan: methodology. Yunxu Yang: project administration, writing – review & editing.

Conflicts of interest

There are no conflicts to declare.

Acknowledgements

This research was supported by the National Science Foundation of China (No. 21575012), the Natural Science Foundation of Beijing (No. 2212010), and the Fundamental Research Funds for the Central Universities (FRF-BR-19-003B).

Notes and references

1 Z. M. Zhang, C. Y. Zhao, J. Ma and G. K. Li, *Analyst*, 2014, **139**, 3614–3621.
2 C. Doroftei, *Sens. Actuators, B*, 2016, **231**, 793–799.
3 S. El Sayed, L. M. Pascual, R. Licchelli, S. Gil Martinez-Manez, A. M. Costero and F. Sancenon, *ACS Appl. Mater. Interfaces*, 2016, **8**, 14318–14322.
4 M. Q. Yang and J. H. He, *Sens. Actuators, B*, 2016, **228**, 486–490.
5 (*a*) P. Spanel, D. Smith, T. A. Holland, W. Al-Singary and J. B. Elder, *Rapid Commun. Mass Spectrom.*, 1999, **13**, 1354–1359; (*b*) S. Kato, P. J. Burke, T. H. Koch and V. M. Bierbaum, *Anal. Chem.*, 2001, **73**, 2992–2997; (*c*) G. R. Mohlmann, *Appl. Spectrosc.*, 1985, **39**, 98–101.
6 J. R. Hopkins, T. Still, S. Al-Haider, I. R. Fisher, A. C. Lewis and P. W. Seakins, *Atmos. Environ.*, 2003, **37**, 2557.
7 (*a*) X. Y. Lai, P. Li, T. L. Yang, J. C. Tu and P. Xue, *Scr. Mater.*, 2012, **67**, 293–296; (*b*) F. Fang, L. Bai, D. S. Song, H. P. Yang, X. M. Sun, H. Y. Sun and J. Zhu, *Sensors*, 2015, **15**, 20086–20096; (*c*) E. X. Chen, H. Yang and J. Zhang, Zeolitic imidazolate framework as formaldehyde gas sensor, *Inorg. Chem.*, 2014, **53**, 5411–5413.
8 T. F. Brewer and C. J. Chang, *J. Am. Chem. Soc.*, 2015, **137**, 10886–10889.
9 H. Song, S. Rajendiran, N. Kim, S. K. Jeong, E. Koo, G. Park, T. D. Thangadurai and S. Yoon, *Tetrahedron Lett.*, 2012, **53**, 4913–4916.
10 J. B. Kevin, R. W. Ryan, F. B. Thomas, B.-B. Guillermo, W. Niek, B. P. Lucas, J. P. Ketan and J. C. Christopher, *J. Am. Chem. Soc.*, 2017, **139**, 5338–5350.
11 A. Roth, H. Li, C. Anorma and J. Chan, *J. Am. Chem. Soc.*, 2015, **137**, 10890–10893.
12 Z. Li, Y. Xu, H. Zhu and Y. Qian, *Chem. Sci.*, 2017, **8**, 5616–5621.
13 T. F. Brewer, G. Burgos-Barragan, N. Wit, K. J. Patel and C. J. Chang, *Chem. Sci.*, 2017, **8**, 4073–4081.
14 C. Liu, C. Shi, H. Li, W. Du, Z. Li, L. Wei and M. Yu, *Sens. Actuators, B*, 2015, **219**, 185–191.
15 W. Zhou, H. Dong, H. Yan, C. Shi, M. Yu, L. Wei and Z. Li, *Sens. Actuators, B*, 2015, **209**, 664–669.
16 S. Nandi, H. Reinsch, S. Banesh, N. Stock, V. Trivedi and S. Biswas, *Dalton Trans.*, 2017, **46**, 12856–12864.
17 A. Buragohain and S. Biswas, *CrystEngComm*, 2016, **18**, 4374–4381.
18 Z. Bao, G. Chang, H. Xing, R. Krishna, Q. Ren and B. Chen, *Energy Environ. Sci.*, 2016, **9**, 3612–3641.
19 R. Dalapati, B. Sakthivel, A. Dhakshinamoorthy, A. Buragohain, A. Bhunia, C. Janiak and S. Biswas, *CrystEngComm*, 2016, **18**, 7855–7864.
20 R. Dalapati, B. Sakthivel, M. K. Ghosalya, A. Dhakshinamoorthy and S. Biswas, *CrystEngComm*, 2017, **19**, 5915–5925.
21 A. R. Chowdhuri, D. Bhattacharya and S. K. Sahu, *Dalton Trans.*, 2016, **45**, 2963–2973.
22 S. Nandi, E. Sharma, V. Trivedi and S. Biswas, *Inorg. Chem.*, 2018, **57**, 15149–15157.
23 K. Vellingiri, A. Deep, K.-H. Kim, D. W. Boukhvalov, P. Kumar and Q. Yao, *Sens. Actuators, B*, 2017, **241**, 938–948.
24 C. Li, J. Huang, H. Zhu, L. Liu, Y. Feng, G. Hu and X. Yu, *Sens. Actuators, B*, 2017, **253**, 275–282.
25 J. N. Hao and B. Yan, *Nanoscale*, 2016, **8**, 12047–12053.
26 M. W. Li, A. Shen, Y. Q. Liang, H. Zhen, X. H. Hao, X. L. Liu, X. C. Sun and Y. X. Yang, *Anal. Methods*, 2020, **12**, 3748–3755.
27 B. L. Chen, Y. Yang, F. Zapata, G. D. Qian and E. B. Lobkovsky, *Adv. Mater.*, 2007, **19**, 1693–1696.
28 L. V. Meyer, F. Schonfeld and K. Muller-Buschbaum, *Chem. Commun.*, 2014, **50**, 8093–8108.
29 S. S. Nagarkar, B. Joarder, A. K. Chaudhari, S. S. Mukherjee and K. Ghosh, *Angew. Chem.*, 2013, **52**, 2881–2885.
30 J. M. Zhou, H. H. Li, H. M. Li, W. Shi and P. Cheng, *Adv. Mater.*, 2015, **27**, 7072–7077.
31 H. L. Guo, Y. Z. Zhu, S. L. Qiu, J. A. Lercher and H. J. Zhang, *Adv. Mater.*, 2010, **22**, 4190–4192.

32 Z. S. Dou, J. C. Yu, Y. J. Cui, Y. Yang, Z. Y. Wang, D. R. Yang and G. D. Qian, *J. Am. Chem. Soc.*, 2014, **136**, 5527–5530.
33 M. J. Dong, M. Zhao, S. Ou, C. Zou and C. D. Wu, *Angew. Chem.*, 2014, **126**, 1601–1605.
34 X. Liu, W. T. Fu and E. Bouwman, *Chem. Commun.*, 2016, **52**, 6926–6929.
35 I. Hod, W. J. Bury, D. M. Karlin, P. D. Deria, C. W. Kung, M. J. Katz, M. So, B. Klahr, D. Jin, Y. W. Chung, T. W. Odom, O. K. Farha and J. T. Hupp, *Adv. Mater.*, 2014, **26**, 6295–6300.
36 W. J. Li, J. F. Feng, S. Y. Gao and R. Cao, *Chem. Commun.*, 2016, **52**, 3951–3954.
37 W. T. Yang, J. Feng and H. J. Zhang, *J. Mater. Chem.*, 2012, **22**, 6819–6823.
38 A. T. Nikolina, A. Manuel, A. Cristina, C.-R. Manuel, M. L. Alejandro, L.-M. Juan Manuel, R.-C. Enrique and J. B. Teresa, *ACS Appl. Bio Mater.*, 2018, **1**, 693–707.
39 C. H. Li, L. Zhu, W. X. Yang, X. He, S. L. Zhao, X. S. Zhang, W. Z. Tang, J. L. Wang, T. L. Yue and Z. H. Li, *J. Agric. Food Chem.*, 2019, **67**, 1277–1283.
40 H. X. Guo, Y. H. Zhang, Z. S. Zheng, H. B. Lin and Y. F. Zhang, *Talanta*, 2017, **170**, 146–151.
41 H. Q. Yin, X. Y. Wang and X. B. Yin, *J. Am. Chem. Soc.*, 2019, **141**, 15166–15173.
42 J.-N. Hao and B. Yan, *Nanoscale*, 2016, **8**, 12047–12053.
43 L. X. Shang and F. Y. Piao, Environmental pollutants, in *Reproductive and developmental toxicity of environmental hazards, ISBN 9787534984402*, Henan Science and Technology Press, Zhengzhou, China, 2017, p. 190.